

Studying of $B_s \rightarrow K^{(*)-}\pi^+$, $K^{(*)-}\rho^+$ decays within supersymmetry

Ru-Min Wang^{1*}, Yuan-Guo Xu^{2†}

¹*College of Physics and Electronic Engineering, Xinyang Normal University, Xinyang, Henan 464000, China*

²*Institute of Particle Physics, Huazhong Normal University, Wuhan, Hubei 430079, China*

July 20, 2010

Abstract

Recent results from CDF Collaboration favor a large CP asymmetry in $B_s \rightarrow K^-\pi^+$ decay, while the Standard Model prediction is very small. Moreover, the measurement of its branching ratio is lower than the Standard Model prediction based on the QCD factorization. We compute the gluino-mediated supersymmetry contributions to $B_s \rightarrow K^{(*)-}\pi^+, K^{(*)-}\rho^+$ decays in the frame of the mass insertion method, and find that for $\frac{m_{\tilde{g}}^2}{m_{\tilde{q}}^2} \leq 2$, the theoretical predictions including the LR and RL mass insertion contributions are compatible with the measurements of $B_s \rightarrow K^-\pi^+$ decay and $B^0 - \bar{B}^0$ mixing within 2σ ranges. Using the constrained LR and RL mass insertion parameter spaces, we explore the supersymmetry mass insertion effects on the branching ratios, the direct CP asymmetries and the polarization fractions in $B_s \rightarrow K^{*-}\pi^+, K^-\rho^+, K^{*-}\rho^+$ decays. We find the constrained LR and RL insertions can provide sizable contributions to the branching ratios of $B_s \rightarrow K^{*-}\pi^+, K^{(*)-}\rho^+$ as well as the direct CP asymmetry and the longitudinal polarization of $B_s \rightarrow K^{*-}\rho^+$ decay without conflict with all related data within 2σ ranges. Near future experiments at Fermi Lab and CERN LHC-b can test our predictions and shrink/reveal the mass insertion parameter spaces.

PACS Numbers: 12.60.Jv, 12.15.Ji, 12.38.Bx, 13.25.Hw

*E-mail: ruminwang@gmail.com

†E-mail: yuangx@iopp.ccnu.edu.cn

1 Introduction

In the recent ten years, the successful running of B factories BABAR and Belle has provided rich experimental data for B^\pm and B^0 , which has confirmed the Kobayashi-Maskawa CP asymmetry mechanism in the Standard Model (SM) and also shown hints for new physics (NP). Among the rich phenomena of B decays, the decay modes of B mesons into pairs of charmless mesons are the known effective probes of the CP violation in the SM and are sensitive to potential NP scenarios beyond the SM. The two body charmless B_s decays will play the similar role in studying the CP asymmetries (CPA), determining CKM matrix elements and constraining/searching for the indirect effects of various NP scenarios. Recently the CDF Collaboration at Fermilab Tevatron has made the first measurement of charmless two-body $B_s \rightarrow K^-\pi^+$ decay [1–4]

$$\begin{aligned}\mathcal{B}(B_s \rightarrow K^-\pi^+) &= (5.0 \pm 0.7 \pm 0.8) \times 10^{-6}, \\ \mathcal{A}_{CP}^{dir}(B_s \rightarrow K^-\pi^+) &= 0.39 \pm 0.15 \pm 0.08.\end{aligned}\quad (1)$$

The measurement is important for understanding B_s physics, and also implies that many B_s decay modes could be precisely measured at the LHC-b.

Compared with the theoretical predictions for these quantities in Refs. [5–7], based on the QCD factorization (QCDF) [8], the perturbative QCD (PQCD) [9], and the soft-collinear effective theory (SCET) [10], respectively, one would find the experimental measurement of this branching ratio agrees with the SM predictions with SCET [5], but lower than the predictions with QCDF and PQCD [6, 7]. For the CDF measurement of $\mathcal{A}_{CP}^{dir}(B_s \rightarrow K^-\pi^+)$, its central value favors a large CP violation in $B_s \rightarrow K^-\pi^+$ decay (different from 0 at 2.3σ), although it is also compatible with zero. In Refs. [11, 12], a robust test of the SM or a probe of NP is suggested by comparison of the direct CPA asymmetry in $B_s \rightarrow K^-\pi^+$ decay.

The decays $B_s \rightarrow K^{(*)-}\pi^+$, $K^{(*)-}\rho^+$ have been extensively studied in the literatures (for example, Refs. [5–7, 11–17]). The tree-dominated decays $B_s \rightarrow K^{(*)-}\pi^+$, $K^{(*)-}\rho^+$ are induced by $\bar{b} \rightarrow \bar{u}u\bar{d}$ transition at the quark level, where the direct CPA are expected to be small in the SM. At present, among many measurements in the similar modes of $B_{u,d}$ decays, several discrepancies with the SM predictions have appeared in tree-dominated $\bar{b} \rightarrow \bar{u}u\bar{q}$ ($q = s, d$) processes, for example, $B \rightarrow \pi\pi, \pi K$ puzzles [18–22]. Although the discrepancies are not statistically significant, there is an unifying similarity pointing to NP (for example, Refs. [23–

25]). There could be also potential NP contributions in $B_s \rightarrow K^{(*)-}\pi^+$, $K^{(*)-}\rho^+$ decays. The measurement given in Eq. (1) will afford an opportunity to search/constrain NP scenarios beyond the SM.

Supersymmetry (SUSY) is an extension of the SM which emerges as one of the most promising candidates for NP beyond the SM. In SUSY, supersymmetric version of the SM contributes to the Flavor Change Natural Current (FCNC) processes. The flavor-changing in these processes is intrinsically tied to usual CKM-induced flavor-changing of the SM (If that were the only new source of flavor physics, we would say the model is minimally flavor violating). But general SUSY is not minimally flavor violation. For general SUSY, a new source of flavor violation is introduced by the squark mass matrices, which usually can not be diagonalized on the same basis as the quark mass matrices. This means gluinos (and other gaugios) will have flavor-changing couplings to quarks and squarks, which implies the FCNCs are mediated by gluinos and thus have strong interaction strength. In order to analyze the phenomenology of non-minimally flavor violating interactions in general SUSY framework, it is helpful to rotate the effects so that they occur in squark propagators rather than in couplings, and to parameterize them in terms of dimensionless mass insertion (MI) parameters $(\delta_{AB}^{u,d})_{ij}$ with $(A, B) = (L, R)$ and $(i, j = 1, 2, 3)$. In this paper, we work in the usual MI approximation [26, 27], and consider $B_s \rightarrow K^{(*)-}\pi^+$, $K^{(*)-}\rho^+$ decays, in general SUSY models, where flavor violation due to the gluino mediation can be important. The chargino-stop and the charged Higgs-top loop contributions are parametrically suppressed relative to the gluino contributions, and thus are ignored following [27–30]. In our work, we also discuss the implications of $B^0 - \bar{B}^0$ mixing since the relevant MI parameters, that affect $B_s \rightarrow K^{(*)-}\pi^+$, $K^{(*)-}\rho^+$ decays, enter also in $B^0 - \bar{B}^0$ mixing. We consider the LR, RL, LL and RR four kinds of the MIs. We find that for $\frac{m_g^2}{m_q^2} \leq 2$, our predictions including the LR or RL MI effects are compatible with the measurements of $B_s \rightarrow K^-\pi^+$ decay and $B^0 - \bar{B}^0$ mixing within 2σ ranges, and the constrained both LR and RL MIs could significantly affect the polarization fractions of $B_s \rightarrow K^{*-}\rho^+$ decay. While the constrained LL and RR insertions from $B^0 - \bar{B}^0$ mixing can not explain the possible large CP asymmetry and the small branching ratio of $B_s \rightarrow K^-\pi^+$ because of lacking the gluino mass enhancement in the decay. Therefore, with the ongoing B -physics at Tevatron, in particular with the onset of the LHC-b experiment, we expect a wealth of B_s decay data and measurements of

these observables could restrict or reveal the parameter spaces of the LR and RL insertions in the near future.

The paper is arranged as follows. In Sec. 2, the relevant formulas for $B_s \rightarrow K^{(*)-}\pi^+$, $K^{(*)-}\rho^+$ decays and $B^0 - \bar{B}^0$ mixing are presented. We also tabulate the theoretical inputs in this section. Sec. 3 deals with the numerical results. Using our constrained MI parameter spaces from $B_s \rightarrow K^-\pi^+$ decay and $B^0 - \bar{B}^0$ mixing, we explore the MI effects on the other observable quantities, which have not been measured yet in $B_s \rightarrow K^{(*)-}\pi^+$, $K^{(*)-}\rho^+$ decays. Sec. 4 contains our summary and conclusion.

2 The theoretical frame

2.1 The decay amplitudes for $B_s \rightarrow K^{(*)-}\pi^+$, $K^{(*)-}\rho^+$ decays

2.1.1 The decay amplitudes in the SM

In the SM, the low energy effective Hamiltonian for the $b \rightarrow u\bar{u}d$ transition at the scale $\mu \sim m_b$ is given by [31]

$$\mathcal{H}_{eff}^{SM}(\Delta B = 1) = \frac{G_F}{\sqrt{2}} \sum_{p=u,c} \lambda_p \left(C_1^{SM} Q_1^p + C_2^{SM} Q_2^p + \sum_{i=3}^{10} C_i^{SM} Q_i + C_{7\gamma}^{SM} Q_{7\gamma} + C_{8g}^{SM} Q_{8g} \right) + \text{h.c.}, \quad (2)$$

here $\lambda_p = V_{pb}V_{pd}^*$ with $p \in \{u, c\}$ are CKM factors, the Wilson coefficients within the SM C_i^{SM} can be found in Ref. [31], and the relevant operators Q_i are given as

$$\begin{aligned} Q_1^p &= (\bar{p}_\alpha \gamma^\mu L b_\alpha)(\bar{d}_\beta \gamma_\mu L p_\beta), & Q_2^p &= (\bar{p}_\alpha \gamma^\mu L b_\beta)(\bar{d}_\beta \gamma_\mu L p_\alpha), \\ Q_3 &= (\bar{d}_\alpha \gamma^\mu L b_\alpha) \sum_{q'} (\bar{q}'_\beta \gamma_\mu L q'_\beta), & Q_4 &= (\bar{d}_\beta \gamma^\mu L b_\alpha) \sum_{q'} (\bar{q}'_\alpha \gamma_\mu L q'_\beta), \\ Q_5 &= (\bar{d}_\alpha \gamma^\mu L b_\alpha) \sum_{q'} (\bar{q}'_\beta \gamma_\mu R q'_\beta), & Q_6 &= (\bar{d}_\beta \gamma^\mu L b_\alpha) \sum_{q'} (\bar{q}'_\alpha \gamma_\mu R q'_\beta), \\ Q_7 &= \frac{3}{2} (\bar{d}_\alpha \gamma^\mu L b_\alpha) \sum_{q'} e_{q'} (\bar{q}'_\beta \gamma_\mu R q'_\beta), & Q_8 &= \frac{3}{2} (\bar{d}_\beta \gamma^\mu L b_\alpha) \sum_{q'} e_{q'} (\bar{q}'_\alpha \gamma_\mu R q'_\beta), \\ Q_9 &= \frac{3}{2} (\bar{d}_\alpha \gamma^\mu L b_\alpha) \sum_{q'} e_{q'} (\bar{q}'_\beta \gamma_\mu L q'_\beta), & Q_{10} &= \frac{3}{2} (\bar{d}_\beta \gamma^\mu L b_\alpha) \sum_{q'} e_{q'} (\bar{q}'_\alpha \gamma_\mu L q'_\beta), \\ Q_{7\gamma} &= \frac{e}{8\pi^2} m_b \bar{d}_\alpha \sigma^{\mu\nu} R b_\alpha F_{\mu\nu}, & Q_{8g} &= \frac{g_s}{8\pi^2} m_b \bar{d}_\alpha \sigma^{\mu\nu} R T_{\alpha\beta}^a b_\beta G_{\mu\nu}^a, \end{aligned} \quad (3)$$

where α and β are color indices, and $L(R) = (1 - (+)\gamma_5)$.

With the weak effective Hamiltonian given in Eq. (2), one can write the decay amplitudes for the relevant two-body hadronic $B \rightarrow M_1 M_2$ decays as

$$\begin{aligned}\mathcal{A}^{SM}(B \rightarrow M_1 M_2) &= \langle M_1 M_2 | \mathcal{H}_{eff}^{SM}(\Delta B = 1) | B \rangle \\ &= \sum_p \sum_i \lambda_p C_i^{SM}(\mu) \langle M_1 M_2 | Q_i(\mu) | B \rangle.\end{aligned}\quad (4)$$

The essential theoretical difficulty for obtaining the decay amplitude arises from the evaluation of hadronic matrix elements $\langle M_1 M_2 | Q_i(\mu) | B \rangle$, for which we will employ the QCDF [8] throughout this paper. We will use the QCDF amplitudes of these decays derived in the comprehensive papers [6, 13] as inputs for the SM amplitudes.

2.1.2 SUSY effects in the decays

In SUSY extension of the SM with conserved R-parity, the potentially most important contributions to Wilson coefficients of penguins in the effective Hamiltonian arise from strong-interaction penguin and box diagrams with gluino-squark loops. They can contribute to the FCNC processes because the gluinos have flavor-changing coupling to the quark and squark eigenstates. In general SUSY, we only consider these potentially large gluino box and penguin contributions and neglect a multitude of other diagrams, which are parametrically suppressed by small electroweak gauge coupling [27–30]. The relevant Wilson coefficients of $b \rightarrow u\bar{u}d$ process due to the gluino box or penguin diagram involving the LL and LR insertions are given (at the scale $\mu \sim m_W \sim m_{\tilde{q}}$) by [27, 32–34]

$$\begin{aligned}C_3^{SUSY}(m_{\tilde{q}}) &= -\frac{\alpha_s^2(m_{\tilde{q}})}{2\sqrt{2}G_F\lambda_t m_{\tilde{q}}^2} \left(-\frac{1}{9}B_1(x) - \frac{5}{9}B_2(x) - \frac{1}{18}P_1(x) - \frac{1}{2}P_2(x) \right) (\delta_{LL}^d)_{13}, \\ C_4^{SUSY}(m_{\tilde{q}}) &= -\frac{\alpha_s^2(m_{\tilde{q}})}{2\sqrt{2}G_F\lambda_t m_{\tilde{q}}^2} \left(-\frac{7}{3}B_1(x) + \frac{1}{3}B_2(x) + \frac{1}{6}P_1(x) + \frac{3}{2}P_2(x) \right) (\delta_{LL}^d)_{13}, \\ C_5^{SUSY}(m_{\tilde{q}}) &= -\frac{\alpha_s^2(m_{\tilde{q}})}{2\sqrt{2}G_F\lambda_t m_{\tilde{q}}^2} \left(\frac{10}{9}B_1(x) + \frac{1}{18}B_2(x) - \frac{1}{18}P_1(x) - \frac{1}{2}P_2(x) \right) (\delta_{LL}^d)_{13}, \\ C_6^{SUSY}(m_{\tilde{q}}) &= -\frac{\alpha_s^2(m_{\tilde{q}})}{2\sqrt{2}G_F\lambda_t m_{\tilde{q}}^2} \left(-\frac{2}{3}B_1(x) + \frac{7}{6}B_2(x) + \frac{1}{6}P_1(x) + \frac{3}{2}P_2(x) \right) (\delta_{LL}^d)_{13}, \\ C_{7\gamma}^{SUSY}(m_{\tilde{q}}) &= \frac{8\pi\alpha_s(m_{\tilde{q}})}{9\sqrt{2}G_F\lambda_t m_{\tilde{q}}^2} \left[(\delta_{LL}^d)_{13} M_4(x) - (\delta_{LR}^d)_{13} \left(\frac{m_{\tilde{q}}}{m_b} \right) 4B_1(x) \right], \\ C_{8g}^{SUSY}(m_{\tilde{q}}) &= -\frac{2\pi\alpha_s(m_{\tilde{q}})}{\sqrt{2}G_F\lambda_t m_{\tilde{q}}^2} \left[(\delta_{LL}^d)_{13} \left(\frac{3}{2}M_3(x) - \frac{1}{6}M_4(x) \right) \right. \\ &\quad \left. + (\delta_{LR}^d)_{13} \left(\frac{m_{\tilde{q}}}{m_b} \right) \frac{1}{6} (4B_1(x) - 9x^{-1}B_2(x)) \right],\end{aligned}\quad (5)$$

where $x \equiv m_{\tilde{q}}^2/m_q^2$, and the loop functions $B_i(x)$, $P_i(x)$, $M_i(x)$ can be found in Ref. [32]. For the RR and RL insertions, we have additional operators $\tilde{Q}_{i=3\dots 6, 7\gamma, 8g}$ that are obtained by $L \leftrightarrow R$ in the SM operators given in Eq. (3). The associated Wilson coefficients $\tilde{C}_{i=3\dots 6, 7\gamma, 8g}^{SUSY}$ are either dominated by their expressions as above with the replacement $L \leftrightarrow R$. The remaining coefficients are either dominated by their SM ($C_{1,2}$) or are electroweak penguins ($C_{7\dots 10}$) and therefore small.

The SUSY Wilson coefficients at low energy $C_i^{SUSY}(\mu \sim m_b)$ can be obtained from $C_i^{SUSY}(m_{\tilde{q}})$ in Eq. (5) by using the renormalization group equation as discussed in Ref. [31]

$$C(\mu) = U_5(\mu, m_{\tilde{q}})C(m_{\tilde{q}}), \quad (6)$$

where C is the 6×1 column vector of the Wilson coefficients and $U_5(\mu, m_{\tilde{q}})$ is the five-flavor 6×6 evolution matrix. The detailed explicitness of $U_5(\mu, m_{\tilde{q}})$ is given in Ref. [31]. The coefficients $C_{7\gamma}^{SUSY}$ and C_{7g}^{SUSY} at the $\mu \sim m_b$ scale are given by [35, 36]

$$\begin{aligned} C_{7\gamma}^{SUSY}(\mu) &= \eta^2 C_{7\gamma}^{SUSY}(m_{\tilde{q}}) + \frac{8}{3}(\eta - \eta^2) C_{8g}^{SUSY}(m_{\tilde{q}}), \\ C_{8g}^{SUSY}(\mu) &= \eta C_{8g}^{SUSY}(m_{\tilde{q}}), \end{aligned} \quad (7)$$

where $\eta = \left(\frac{\alpha_s(m_{\tilde{q}})}{\alpha_s(m_t)}\right)^{\frac{2}{21}} \left(\frac{\alpha_s(m_t)}{\alpha_s(m_b)}\right)^{\frac{2}{23}}$.

2.1.3 The total decay amplitudes

For the LL and LR insertion, the NP effective operators have the same chirality with ones of the SM, so the total decays amplitudes can be obtained from the SM ones in Refs. [6, 13] by replacing

$$C_i^{SM} \rightarrow C_i^{SM} + C_i^{SUSY}. \quad (8)$$

For RL and RR insertion, the NP effective operators have the opposite chirality with the SM ones, and we can get the corresponding decay amplitudes from the SM decay amplitudes by following replacements [37]

$$C_i^{SM} \rightarrow C_i^{SM} - \tilde{C}_i^{SUSY}, \quad (9)$$

for $A(B_s \rightarrow K^- \pi^+)$ and $A_{0,\parallel}(B_s \rightarrow K^{*-} \rho^+)$, as well as

$$C_i^{SM} \rightarrow C_i^{SM} + \tilde{C}_i^{SUSY}, \quad (10)$$

for $A(B_s \rightarrow K^{*-} \pi^+)$, $A(B_s \rightarrow K^- \rho^+)$ and $A_\perp(B_s \rightarrow K^{*-} \rho^+)$.

Then the total branching ratios read

$$\mathcal{B}(B_s \rightarrow M_1 M_2) = \frac{\tau_{B_s} |p_c|}{8\pi m_{B_s}^2} |\mathcal{A}(B_s \rightarrow M_1 M_2)|^2, \quad (11)$$

where τ_{B_s} is the B_s lifetime, $|p_c|$ is the center of mass momentum in the center of mass frame of B_s meson.

The direct CP asymmetry is defined as

$$\mathcal{A}_{CP}^{dir}(B_s \rightarrow f) = \frac{\mathcal{B}(\bar{B}_s \rightarrow \bar{f}) - \mathcal{B}(B_s \rightarrow f)}{\mathcal{B}(\bar{B}_s \rightarrow \bar{f}) + \mathcal{B}(B_s \rightarrow f)}. \quad (12)$$

In the $B_s \rightarrow VV$ decay, the two vector mesons have the same helicity, therefore three different polarization states are possible, one longitudinal and two transverse, and we define the corresponding amplitudes as $\mathcal{A}_{0,\pm}$. Transverse ($\mathcal{A}_{\parallel,\perp}$) and helicity (\mathcal{A}_\pm) amplitudes are related by $\mathcal{A}_{\parallel,\perp} = \frac{\mathcal{A}_+ \pm \mathcal{A}_-}{\sqrt{2}}$. Then we have

$$|\mathcal{A}(B_s \rightarrow VV)|^2 = |\mathcal{A}_0|^2 + |\mathcal{A}_+|^2 + |\mathcal{A}_-|^2 = |\mathcal{A}_0|^2 + |\mathcal{A}_\parallel|^2 + |\mathcal{A}_\perp|^2. \quad (13)$$

The longitudinal(transverse) polarization fraction $f_L(f_\perp)$ are defined by

$$f_{L,\perp}(B_s \rightarrow VV) = \frac{\Gamma_{L,\perp}}{\Gamma} = \frac{|\mathcal{A}_{0,\perp}|^2}{|\mathcal{A}_0|^2 + |\mathcal{A}_\parallel|^2 + |\mathcal{A}_\perp|^2}. \quad (14)$$

2.2 Effective Hamiltonian for $B^0 - \bar{B}^0$ mixing

The most general $B^0 - \bar{B}^0$ mixing is described by the effective Hamiltonian [38]

$$\mathcal{H}_{eff}(\Delta B = 2) = \sum_{i=1}^5 C'_i Q'_i + \sum_{i=1}^3 \tilde{C}'_i \tilde{Q}'_i + h.c., \quad (15)$$

with

$$\begin{aligned} Q'_1 &= (\bar{d}\gamma^\mu P_L b)_1 (\bar{d}\gamma_\mu P_L b)_1, \\ Q'_2 &= (\bar{d}P_L b)_1 (\bar{d}P_L b)_1, \\ Q'_3 &= (\bar{d}P_L b)_8 (\bar{d}P_L b)_8, \\ Q'_4 &= (\bar{d}P_L b)_1 (\bar{d}P_R b)_1, \\ Q'_5 &= (\bar{d}P_L b)_8 (\bar{d}P_R b)_8, \end{aligned} \quad (16)$$

where $P_{L(R)} = (1 - (+)\gamma_5)/2$ and the operators $\tilde{Q}'_{1,2,3}$ are obtained from $Q'_{1,2,3}$ by the exchange $L \leftrightarrow R$. The hadronic matrix elements, taking into account for renormalization effects, are defined as

$$\begin{aligned}\langle \bar{B}^0 | Q'_1(\mu) | B^0 \rangle &= \frac{2}{3} m_{B_d}^2 f_{B_d}^2 B_1(\mu), \\ \langle \bar{B}^0 | Q'_2(\mu) | B^0 \rangle &= -\frac{5}{12} m_{B_d}^2 f_{B_d}^2 S_{B_d} B_2(\mu), \\ \langle \bar{B}^0 | Q'_3(\mu) | B^0 \rangle &= \frac{1}{12} m_{B_d}^2 f_{B_d}^2 S_{B_d} B_3(\mu), \\ \langle \bar{B}^0 | Q'_4(\mu) | B^0 \rangle &= \frac{1}{2} m_{B_d}^2 f_{B_d}^2 S_{B_d} B_4(\mu), \\ \langle \bar{B}^0 | Q'_5(\mu) | B^0 \rangle &= \frac{1}{6} m_{B_d}^2 f_{B_d}^2 S_{B_d} B_5(\mu),\end{aligned}\quad (17)$$

with $S_{B_d} = \left(\frac{m_{B_d}}{\overline{m}_b(\overline{m}_b) + \overline{m}_d(\overline{m}_b)} \right)^2$.

The Wilson coefficients C'_i receive contributions from both the SM and the SUSY loops: $C'_i \equiv C'^{SM}_i + C'^{SUSY}_i$. In the SM, the $t - W$ box diagram generates only contribution to the operator Q'_1 , and the corresponding Wilson coefficient C'^{SM}_1 at the m_b scale is [31]

$$C'^{SM}_1(m_b) = \frac{G_F^2}{4\pi^2} m_W^2 (V_{td} V_{tb}^*)^2 \eta_{2B} S_0(x_t) [\alpha_s(m_b)]^{-6/23} \left[1 + \frac{\alpha_s(m_b)}{4\pi} J_5 \right], \quad (18)$$

where $x_t = m_t^2/m_W^2$ and η_{2B} is the QCD correction.

The gluino-mediated SUSY contributions to $B^0 - \bar{B}^0$ mixing and 2β in the MI approximation have been extensively studied (for example, Refs. [38, 40–42]). In general SUSY models, there are new contributions to $B^0 - \bar{B}^0$ mixing from the gluino-squark box diagrams, and the corresponding Wilson coefficients C'^{SUSY}_i (at the $m_{\tilde{q}}$ scale) are given by [27–30]

$$\begin{aligned}C'^{SUSY}_1(m_{\tilde{q}}) &= -\frac{\alpha_s^2}{216 m_{\tilde{q}}^2} (24x f_6(x) + 66 \tilde{f}_6(x)) (\delta_{LL}^d)_{13}^2, \\ C'^{SUSY}_2(m_{\tilde{q}}) &= -\frac{\alpha_s^2}{216 m_{\tilde{q}}^2} 204x f_6(x) (\delta_{RL}^d)_{13}^2, \\ C'^{SUSY}_3(m_{\tilde{q}}) &= \frac{\alpha_s^2}{216 m_{\tilde{q}}^2} 36x f_6(x) (\delta_{RL}^d)_{13}^2, \\ C'^{SUSY}_4(m_{\tilde{q}}) &= -\frac{\alpha_s^2}{216 m_{\tilde{q}}^2} \left[(504x f_6(x) - 72 \tilde{f}_6(x)) (\delta_{LL}^d)_{13} (\delta_{RR}^d)_{13} - 132 \tilde{f}_6(x) (\delta_{LR}^d)_{13} (\delta_{RL}^d)_{13} \right], \\ C'^{SUSY}_5(m_{\tilde{q}}) &= -\frac{\alpha_s^2}{216 m_{\tilde{q}}^2} \left[(24x f_6(x) + 120 \tilde{f}_6(x)) (\delta_{LL}^d)_{13} (\delta_{RR}^d)_{13} - 180 \tilde{f}_6(x) (\delta_{LR}^d)_{13} (\delta_{RL}^d)_{13} \right].\end{aligned}\quad (19)$$

The loop functions $f_6(x)$, $\tilde{f}_6(x)$ can be found in Ref. [32]. The other Wilson coefficients $\tilde{C}'_{1,2,3}^{SUSY}$ are obtained from $C'^{SUSY}_{1,2,3}$ by exchange of $L \leftrightarrow R$.

The SUSY Wilson coefficients at the m_b scale $C_i^{SUSY}(m_b)$ can be obtained by

$$C_r(m_b) = \sum_i \sum_s \left(b_i^{(r,s)} + \eta' c_i^{(r,s)} \right) \eta'^{a_i} C_s(m_{\tilde{q}}), \quad (20)$$

where $\eta' = \alpha_s(m_{\tilde{q}})/\alpha_s(m_t)$. The magic number a_i , $b_i^{(r,s)}$ and $c_i^{(r,s)}$ can be found in Ref. [38]. Renormalization group evolution of $\tilde{C}_{1,2,3}$ is done in the same way as for $C_{1,2,3}$.

In terms of the effective Hamiltonian in Eq. (15), the mixing amplitude M_{12} read

$$M_{12} = \frac{\langle B^0 | \mathcal{H}_{eff}(\Delta B = 2) | \bar{B}^0 \rangle}{2m_{B_d}}. \quad (21)$$

Then, the B^0 mass difference $\Delta M_d = 2|M_{12}|$, its associated CP phase $2\beta = \arg(M_{12})$, and $S_{\psi K_S} = \sin 2\beta$. Experimental values of ΔM_d and 2β are given by the Heavy Flavor Averaging Group [39]

$$\begin{aligned} \Delta M_d &= 0.507 \pm 0.005 \text{ ps}^{-1}, \\ \sin 2\beta &= 0.68 \pm 0.03. \end{aligned} \quad (22)$$

Above experimental bounds will also be used in our numerical results.

2.3 Input Parameters

The input parameters are collected in Table 1. We have several remarks on the input parameters:

- Wilson coefficients: The SM Wilson coefficients C_i^{SM} are obtained from the expressions in Ref. [31].
- CKM matrix element: For the SM predictions, we use the CKM matrix elements from the Wolfenstein parameters of the latest analysis within the SM in Ref. [44], and for the SUSY predictions, we take the CKM matrix elements in terms of the Wolfenstein parameters of the NP generalized analysis results in Ref. [44].
- Masses of SUSY particles: When we study the SUSY effects, we will consider each possible MI $(\delta_{AB}^d)_{13}$ for $AB = LL, LR, RL, RR$ only one at a time, neglecting the interferences between different insertions products, but keeping their interferences with the SM amplitude. We fix the common squark masses $m_{\tilde{q}} = 500$ GeV and consider three values of $x = 0.25, 1, 4$ (i.e. $m_{\tilde{g}} = 250, 500, 1000$ GeV) in all case.

Table 1: Default values of the input parameters.

$m_W = 80.398 \pm 0.025$ GeV, $m_{B_d} = 5.280$ GeV, $m_{B_s} = 5.366$ GeV, $\tau_{B_s} = (1.472^{+0.024}_{-0.026})$ ps,	
$m_{K^*\pm} = 0.892$ GeV, $m_{K^\pm} = 0.494$ GeV, $m_{\pi^\pm} = 0.140$ GeV, $m_\rho = 0.775$ GeV,	
$m_t = 171.3^{+2.1}_{-1.6}$ GeV, $\overline{m}_b(\overline{m}_b) = (4.20 \pm 0.07)$ GeV, $\overline{m}_u(2\text{GeV}) = (0.0015 \sim 0.0033)$ GeV,	
$\overline{m}_d(2\text{GeV}) = (0.0035 \sim 0.0060)$ GeV, $\overline{m}_s(2\text{GeV}) = (0.105^{+0.025}_{-0.035})$ GeV.	[43]
The Wolfenstein parameters for the SM predictions:	
$A = 0.810 \pm 0.013$, $\lambda = 0.2259 \pm 0.0016$, $\bar{\rho} = 0.154 \pm 0.022$, $\bar{\eta} = 0.342 \pm 0.014$.	
The Wolfenstein parameters for the SUSY predictions:	
$A = 0.810 \pm 0.013$, $\lambda = 0.2259 \pm 0.0016$, $\bar{\rho} = 0.177 \pm 0.044$, $\bar{\eta} = 0.360 \pm 0.031$.	[44]
$f_K = 0.160$ GeV, $f_{K^*} = (0.217 \pm 0.005)$ GeV, $f_{K^*}^\perp = (0.156 \pm 0.010)$ GeV,	
$f_\pi = 0.131$ GeV, $f_\rho = (0.205 \pm 0.009)$ GeV, $f_\rho^\perp = (0.147 \pm 0.010)$ GeV,	
$A_0^{B_s \rightarrow K^*}(0) = 0.360 \pm 0.034$, $A_1^{B_s \rightarrow K^*}(0) = 0.233 \pm 0.022$, $A_2^{B_s \rightarrow K^*}(0) = 0.181 \pm 0.025$,	
$V^{B_s \rightarrow K^*}(0) = 0.311 \pm 0.026$, $F_0^{B_s \rightarrow K}(0) = 0.30^{+0.04}_{-0.03}$	[45, 46]
$f_{B_s} = (0.245 \pm 0.025)$ GeV, $f_{B_d} = (0.200 \pm 0.020)$ GeV, $f_{B_d} \sqrt{\hat{B}_{B_d}} = 0.225 \pm 0.025$ GeV.	[47]
$\lambda_B = (0.46 \pm 0.11)$ GeV.	[48]
$\eta_{2B} = 0.55 \pm 0.01$.	[49]
$\alpha_1^\pi = 0$, $\alpha_2^\pi = 0.20 \pm 0.15$, $\alpha_1^\rho = 0$, $\alpha_2^\rho = 0.1 \pm 0.2$,	
$\alpha_1^K = 0.2 \pm 0.2$, $\alpha_2^K = 0.1 \pm 0.3$, $\alpha_1^{K^*} = 0.06 \pm 0.06$, $\alpha_2^{K^*} = 0.1 \pm 0.2$.	[6, 13]
$B_1^{(d)}(m_b) = 0.87(4) \begin{pmatrix} +5 \\ -4 \end{pmatrix}$, $B_2^{(d)}(m_b) = 0.82(3)(4)$, $B_3^{(d)}(m_b) = 1.02(6)(9)$	
$B_4^{(d)}(m_b) = 1.16(3) \begin{pmatrix} +5 \\ -7 \end{pmatrix}$, $B_5^{(d)}(m_b) = 1.91(4) \begin{pmatrix} +22 \\ -7 \end{pmatrix}$	[50]

3 Numerical results and analysis

Now we are ready to present our numerical results and analysis. First, we will show our estimations in the SM with the parameters listed in Table 1 and compare with the relevant experimental data. Then we will study the SUSY predictions for the branching ratios, the CP asymmetries and the polarization fractions in $B_s \rightarrow K^{(*)-}\pi^+$, $K^{(*)-}\rho^+$ decays. For CPA of $B_s \rightarrow K^{*-}\rho^+$, we will only study the longitudinal direct CP asymmetry ($\mathcal{A}_{CP}^{L,dir}$).

In the SM, the numerical results with 1σ error ranges for the sensitive parameters are presented in Table 2. The detailed error estimates corresponding to the different types of theoretical uncertainties have been already studied in Refs. [6, 13], and our SM results of \mathcal{B} , \mathcal{A}_{CP}^{dir} and f_L are consistent with the ones in Refs. [6, 13]. For the color-allowed tree-dominated decays $B_s \rightarrow K^-\pi^+, K^{*-}\pi^+, K^-\rho^+, K^{*-}\rho^+$, power corrections have limited impact, and the

Table 2: The SM predictions with 1σ error ranges of the input parameters for \mathcal{B} (in units of 10^{-6}), \mathcal{A}_{CP}^{dir} (in units of 10^{-2}) and f_L in $B_s \rightarrow K^{(*)-}\pi^+, K^{(*)-}\rho^+$ decays within QCDF.

Decay modes	\mathcal{B}	\mathcal{A}_{CP}^{dir} ($\mathcal{A}_{CP}^{L,dir}$)	f_L
$B_s \rightarrow K^-\pi^+$	[6.89, 15.67]	[-8.11, -1.44]	
$B_s \rightarrow K^{*-}\pi^+$	[9.03, 18.36]	[-0.64, 2.01]	
$B_s \rightarrow K^-\rho^+$	[14.79, 38.39]	[-1.68, 0.86]	
$B_s \rightarrow K^{*-}\rho^+$	[11.85, 69.69]	[-5.19, -1.02]	[0.87, 0.97]

main sources of theoretical uncertainties in the branching ratios are the CKM matrix elements and the form factors. Their A_{CP}^{dir} and $A_{CP}^{L,dir}$ can be predicted quite precisely, and found to be very small ($\sim 10^{-2}$) due to small penguin amplitudes. The uncertainty of $f_L(B_s \rightarrow K^{*-}\rho^+)$ is mostly due to the uncertainties of different form factors. Comparing the SM predictions in Table 2 with the relevant experimental data in Eq. (1), we may see the present experimental data of the $B_s \rightarrow K^-\pi^+$ decay within 1σ ranges are not consistent with the SM predictions within 1σ error ranges of the input parameters. The experimental data of $\mathcal{A}_{CP}^{dir}(B_s \rightarrow K^-\pi^+)$ are obviously larger than the SM prediction, moreover, the measurement of its branching ratio is lower than the SM prediction based on the QCDF.

Now we turn to the gluino-mediated SUSY contributions to $B_s \rightarrow K^{(*)-}\pi^+, K^{(*)-}\rho^+$ decays in the framework of the MI approximation. These decays are induced by $\bar{b} \rightarrow \bar{u}u\bar{d}$ transition at the quark level, and we consider four kinds of MIs (LL, LR, RL and RR) contributing to $B_s \rightarrow K^{(*)-}\pi^+, K^{(*)-}\rho^+$ decays. In the SM, the very small direct CPA of these decays come from the weak phase of small penguin amplitudes. In order to have nonzero CPA, we need at least two independent amplitudes with different weak phases. In general SUSY models, we are considering, the weak phases reside in the complex MI parameters δ s and appear in the SUSY Wilson coefficients in Eq. (5). These weak phases are odd under a CP transformation.

First, we study constraints on the MI parameters $(\delta_{LL}^d)_{13}$, $(\delta_{LR}^d)_{13}$, $(\delta_{RR}^d)_{13}$ and $(\delta_{RL}^d)_{13}$ from $B_s \rightarrow K^-\pi^+$ decay and $B^0 - \bar{B}^0$ mixing. Using the formulas in Sec. 2.1 and the input parameters in Sec. 2.3, we may obtain the two-body branching ratios and the direct CPA of $B_s \rightarrow K^{(*)-}\pi^+, K^{(*)-}\rho^+$ decays within the framework of SUSY by the QCDF. The mass

difference and CP phase of $B^0 - \bar{B}^0$ mixing are gotten from the formulas in Sec. 2.2 and the input parameters in Sec. 2.3. Noted that we take the relevant CKM matrix elements in terms of the Wolfenstein parameters of the NP generalized analysis results in [44], which is different from the SM predictions. In each of the MI scenarios to be discussed, we vary the mass insertions over the range $|(\delta_{AB}^d)_{13}| \leq 1$ to fully map the parameter space. We then impose experimental constraints from $B_s \rightarrow K^- \pi^+$ decay and $B^0 - \bar{B}^0$ mixing, which are shown in Eq. (1) and Eq. (22), respectively.

For the LL and RR MIs, $|(\delta_{LL}^d)_{13}|$ and $|(\delta_{RR}^d)_{13}|$ are strongly constrained from $B^0 - \bar{B}^0$ mixing [34, 38, 40, 41]. The effects of the constrained LL and RR insertions on $B_s \rightarrow K^- \pi^+$ are almost negligible because of lacking the gluino mass enhancement in the decay, and they will not provide any significant effect on $\mathcal{B}(B_s \rightarrow K^- \pi^+)$ and $\mathcal{A}_{CP}^{dir}(B_s \rightarrow K^- \pi^+)$. The current data within 1σ (or 2σ) ranges of $\mathcal{A}_{CP}^{dir}(B_s \rightarrow K^- \pi^+)$ cannot be explained by the LL and RR MIs.

The case of the LR or RL insertion is very different from that of either LL or RR insertion. The LR and RL MIs only generate (chromo)magnetic operators $Q_{7\gamma,8g}$ and $\tilde{Q}_{7\gamma,8g}$, respectively. Especially, the LR and RL insertions are more strongly constrained, since their contributions are enhanced by $m_{\tilde{g}}/m_b$ due to the chirality flip from the gluino in the loop compared with the contribution including the SM one. In these cases, even a small $(\delta_{LR}^d)_{13}$ or $(\delta_{RL}^d)_{13}$ can have large effects in the decays.

We can not get the allowed spaces of the LR and RL insertion parameters which may explain all these data within 1σ ranges given in Eq. (1) and Eq. (22) at the same time. In fact, there is no common allowed parameter space from $\mathcal{B}(B_s \rightarrow K^- \pi^+)$ and $\mathcal{A}_{CP}^{dir}(B_s \rightarrow K^- \pi^+)$ within 1σ ranges. Using the central values of the input parameters and $m_{\tilde{g}} = m_{\tilde{b}} = 500$ GeV, we show the contour plots of $\mathcal{B}(B_s \rightarrow K^- \pi^+)$ and $\mathcal{A}_{CP}^{dir}(B_s \rightarrow K^- \pi^+)$ in the $|(\delta_{LR}^d)_{13}| - \phi_{LR}$ and $|(\delta_{RL}^d)_{13}| - \phi_{RL}$ planes in Fig. 1. We discuss Fig. 1 (a) in detail. Fig. 1 (a) show the contour plot of 1σ error bars of $\mathcal{B}(B_s \rightarrow K^- \pi^+)$ and $\mathcal{A}_{CP}^{dir}(B_s \rightarrow K^- \pi^+)$ in $|(\delta_{LR}^d)_{13}| - \phi_{LR}$ plane. The space between the contour lines of $\mathcal{B}(B_s \rightarrow K^- \pi^+) = 6.1 \times 10^{-6}$ and $\mathcal{B}(B_s \rightarrow K^- \pi^+) = 3.9 \times 10^{-6}$ is the allowed space for $\mathcal{B}(B_s \rightarrow K^- \pi^+)$ within 1σ ranges. The space between the contour lines of $\mathcal{A}_{CP}^{dir}(B_s \rightarrow K^- \pi^+) = 0.56$ and $\mathcal{A}_{CP}^{dir}(B_s \rightarrow K^- \pi^+) = 0.22$ is the allowed space for $\mathcal{A}_{CP}^{dir}(B_s \rightarrow K^- \pi^+)$ within 1σ ranges. From Fig. 1 (a), we can see that there is no intersection

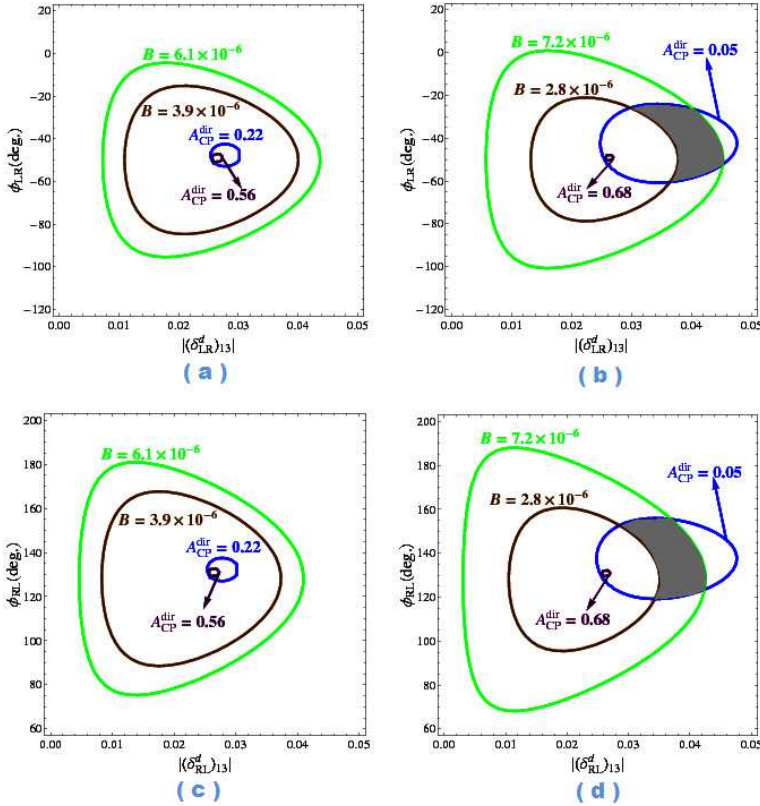


Figure 1: The contour plots of $\mathcal{B}(B_s \rightarrow K^-\pi^+)$ and $\mathcal{A}_{CP}^{dir}(B_s \rightarrow K^-\pi^+)$ in the $|(\delta_{LR}^d)_{13}| - \phi_{LR}$ and $|(\delta_{RL}^d)_{13}| - \phi_{RL}$ planes with the central values of the input parameters and $m_{\tilde{q}} = m_{\tilde{g}} = 500$ GeV. Plots (a) and (c) show the 1σ error-bar of data given in Eq. (1). Plots (b) and (d) show the 2σ error-bar of data given in Eq. (1). ϕ_{AB} denotes the mixing parameters weak phase. Please see text for details.

between the allowed space from $\mathcal{B}(B_s \rightarrow K^-\pi^+)$ and the allowed space from $\mathcal{A}_{CP}^{dir}(B_s \rightarrow K^-\pi^+)$, and the experimental data of $\mathcal{A}_{CP}^{dir}(B_s \rightarrow K^-\pi^+)$ within 1σ give quite strong constraints on $(\delta_{LR}^d)_{13}$. The similar results for the RL insertion are shown in Fig. 1 (c) in $|(\delta_{RL}^d)_{13}| - \phi_{RL}$ plane, and there is also no intersection between the allowed space from $\mathcal{B}(B_s \rightarrow K^-\pi^+)$ within 1σ ranges and the allowed space from $\mathcal{A}_{CP}^{dir}(B_s \rightarrow K^-\pi^+)$ within 1σ ranges.

Then we expand the experimental bounds within 2σ ranges to search for the allowed spaces of the LR and RL MI parameters. As shown in the dark gray ranges of Fig. 1 (b) and (d), there are the allowed spaces for the LR and RL insertion parameters from the data of $B_s \rightarrow K^-\pi^+$ decay within 2σ ranges. Noted that the allowed parameter spaces shown in the dark gray ranges of Fig. 1 (b) and (d) are obtained by using the central values of the input parameters.

The allowed spaces will be enlarged if we consider the theoretical uncertainties of the input parameters. We use the experimental bounds of $B_s \rightarrow K^-\pi^+$ decay and $B^0 - \bar{B}^0$ mixing within 2σ ranges, and take the input parameters within 2σ ranges to obtain the allowed spaces of the LR and RL insertion parameters. The constrained spaces of $(\delta_{LR}^d)_{13}$ and $(\delta_{RL}^d)_{13}$ for $m_{\tilde{q}} = 500$ GeV and different x are demonstrated in Fig. 2, and the corresponding numerical ranges are summarized in Table 3.

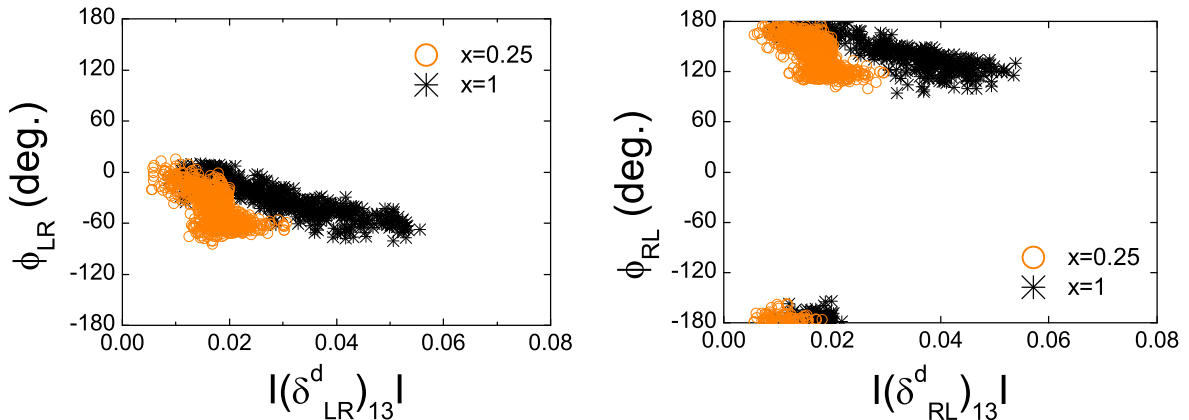


Figure 2: The allowed parameter spaces of the LR and RL MI parameters constrained from $B_s \rightarrow K^-\pi^+$ decay and $B^0 - \bar{B}^0$ mixing at 95% C.L. for the squark mass $m_{\tilde{q}} = 500$ GeV and for the different values of $x = 0.25$ and $x = 1$.

Table 3: Bounds on the LR and RL MI parameters from the measurements of $B_s \rightarrow K^-\pi^+$ decay and $B^0 - \bar{B}^0$ mixing at 95% C.L..

x	$ (\delta_{LR}^d)_{13} $	$\phi_{LR}(\text{deg.})$	$ (\delta_{RL}^d)_{13} $	$\phi_{RL}(\text{deg.})$
0.25	[0.005, 0.031]	[-85, 15]	[0.005, 0.030]	[100, 180] \cup [-180, -158]
1	[0.008, 0.056]	[-81, 10]	[0.008, 0.054]	[94, 180] \cup [-180, -154]

In Fig. 2, we can see the allowed moduli of the LR and RL MI parameters are very sensitive to the values of x , nevertheless the allowed phase ranges of the LR and RL MI parameters are not changed obviously for different x . We find that both moduli and phases of $(\delta_{LR,RL}^d)_{13}$ are strongly constrained by the data of the $B_s \rightarrow K^-\pi^+$ decay within 2σ ranges, since the SM prediction of $\mathcal{A}_{CP}^{dir}(B_s \rightarrow K^-\pi^+)$ with the QCDF is not consistent with the experimental data within 2σ ranges. The lower limits of $|(\delta_{LR,RL}^d)_{13}|$ come from the experimental lower limit of

$\mathcal{A}_{CP}^{dir}(B_s \rightarrow K^-\pi^+)$ within 2σ ranges. In the case of $x = 1$, $\phi_{LR,RL}$ are also constrained by ΔM_d within 2σ ranges, while $\sin 2\beta$ within 2σ ranges doesn't provide any further constraint. It's different in the case of $x = 0.25$, $\phi_{LR,RL}$ are also constrained by $\sin 2\beta$ within 2σ ranges, but ΔM_d within 2σ ranges doesn't provide any further constraint.

It is worth to note that we also study the constrained spaces of $(\delta_{LR}^d)_{13}$ and $(\delta_{RL}^d)_{13}$ in the case of $x = 4$, and we find there is no intersection of the constrained spaces between from $B^0 - B^0$ mixing within 2σ ranges and from $B_s \rightarrow K^-\pi^+$ decay within 2σ ranges. From $B^0 - B^0$ mixing within 2σ ranges, we get $|(\delta_{LR,RL}^d)_{13}| \leq 0.07$, in which $\phi_{LR,RL} \in [-180^\circ, 180^\circ]$ if $|(\delta_{LR,RL}^d)_{13}| \leq 0.03$, and $\phi_{LR,RL} \in [-110^\circ, -45^\circ] \cup [70^\circ, 135^\circ]$ if $|(\delta_{LR,RL}^d)_{13}| \in [0.03, 0.07]$. We obtain $|(\delta_{LR,RL}^d)_{13}| \in [0.03, 0.19]$ from $B_s \rightarrow K^-\pi^+$ decay within 2σ ranges, in which $\phi_{LR} \in [-90^\circ, 5^\circ]$ ($\phi_{RL} \in [-180^\circ, -175^\circ] \cup [90^\circ, 180^\circ]$) if $|(\delta_{LR,RL}^d)_{13}| \in [0.07, 0.19]$, and $\phi_{LR} \in [-40^\circ, 15^\circ]$ ($\phi_{RL} \in [-180^\circ, -165^\circ] \cup [140^\circ, 180^\circ]$) if $|(\delta_{LR,RL}^d)_{13}| \in [0.03, 0.07]$. So there is no common allowed phases between the bounds from $B^0 - B^0$ mixing and the bounds from $B_s \rightarrow K^-\pi^+$ decay in the case of $x = 4$. If $x = 2$, there still are common allowed spaces for the LR and RL MIs. For the LR MI, two very narrow allowed spaces are near $(|(\delta_{LR}^d)_{13}| \approx 0.02, \phi_{LR} \approx 4^\circ)$ and $(|(\delta_{LR}^d)_{13}| \approx 0.04, \phi_{LR} \approx -64^\circ)$. For the RL MI, two very allowed spaces are near $(|(\delta_{RL}^d)_{13}| \approx 0.02, \phi_{RL} \approx -176^\circ)$ and $(|(\delta_{RL}^d)_{13}| \approx 0.04, \phi_{RL} \approx 116^\circ)$.

The relevant upper bounds have been obtained in Refs. [38, 40, 41]. In Ref. [38], $|(\delta_{LR,RL}^d)_{13}| \leq 0.07, 0.08, 0.11$ for $x = 0.25, 1, 4$, respectively, which are constrained by imposing the experimental bounds from ΔM_d and $S_{\psi K_S}$ within 1σ ranges, setting $m_{\tilde{q}} = 500$ GeV and scanning over the CKM phase $\gamma \in [0, 2\pi]$. In Ref. [40], $|(\delta_{LR,RL}^d)_{13}| \leq 0.015$ for $m_{\tilde{g}} = m_{\tilde{q}} = 500$ GeV from ΔM_d and 2β within 2σ ranges. In Ref. [41], $|(\delta_{RL,RL}^d)_{13}| \leq 0.03$ for $m_{\tilde{g}}, m_{\tilde{q}} \leq 600$ GeV from ΔM_d and 2β . In the case of $x = 0.25$ and $x = 1$, comparing with the exist bounds in [38, 40, 41], our upper limits of $|(\delta_{LR,RL}^d)_{13}|$ are at the same order of previous ones, while the lower limits of $|(\delta_{LR,RL}^d)_{13}|$ are also given from $B_s \rightarrow K^-\pi^+$ decay within 2σ ranges. In addition, $\phi_{LR,RL}$ are strongly constrained from $B_s \rightarrow K^-\pi^+$ decay. The allowed space for $x = 4$ case are ruled out by both $B_s \rightarrow K^-\pi^+$ decay and $B^0 - B^0$ mixing together.

Next, we will explore the SUSY effects on the other quantities, which have not been measured yet in $B_s \rightarrow K^{*-}\pi^+, K^{(*)-}\rho^+$ decays, by using the constrained parameter spaces of the LR and LR insertions as shown in Fig. 2. With the expressions for \mathcal{B} , \mathcal{A}_{CP}^{dir} and f_L , we perform a

scan through the input parameters within 2σ ranges and the new constrained SUSY MI parameter spaces, and then the allowed ranges for \mathcal{B} , \mathcal{A}_{CP}^{dir} and f_L are obtained with different SUSY mixing insertion parameter, which satisfy relevant experimental constraints of $B_s \rightarrow K^-\pi^+$ decay given in Eq. (1) and $B^0 - \bar{B}^0$ mixing given in Eq. (22). The numerical results for $B_s \rightarrow K^{*-}\pi^+, K^{(*)-}\rho^+$ with different x value are summarized in Table 4. The corresponding SM predictions with 2σ error ranges of the input parameters are also listed for comparison in the second column of the Table 4. We can see the data of $\mathcal{B}(B_s \rightarrow K^-\pi^+)$ is consistent with the SM prediction of $\mathcal{B}(B_s \rightarrow K^-\pi^+)$ at 95% C.L., nonetheless very close the lower limit of its SM prediction. The data of $\mathcal{A}_{CP}^{dir}(B_s \rightarrow K^-\pi^+)$ is not consistent with its SM prediction at 95% C.L.. From the last four columns of the Table 4, we can see the results are similar for different value of x . In the SUSY predictions of the branching ratios, there are many sources of uncertainties, mainly arising from different form factors, CKM matrix elements, the annihilation contribution, other hadronic parameters of the QCDF, and the constrained MI parameters. The uncertain-

Table 4: The theoretical predictions for \mathcal{B} (in units of 10^{-6}), \mathcal{A}_{CP}^{dir} (in units of 10^{-2}) and f_L in four $B_s \rightarrow K^{(*)-}\pi^+, K^{(*)-}\rho^+$ decays based on general SUSY models with different MI and different x . The corresponding SM predictions with 2σ error ranges of the input parameters are also listed for comparison.

Observables	SM predictions	SUSY values with $(\delta_{LR}^d)_{13}$ for $x = 1$	SUSY values with $(\delta_{LR}^d)_{13}$ for $x = 0.25$	SUSY values with $(\delta_{RL}^d)_{13}$ for $x = 1$	SUSY values with $(\delta_{RL}^d)_{13}$ for $x = 0.25$
$\mathcal{B}(B_s \rightarrow K^-\pi^+)$	[3.32, 24.48]	[2.80, 7.20]	[2.80, 7.20]	[2.80, 7.20]	[2.80, 7.20]
$\mathcal{B}(B_s \rightarrow K^{*-}\pi^+)$	[5.91, 25.80]	[0.25, 30.67]	[0.13, 30.94]	[7.10, 93.54]	[7.53, 93.32]
$\mathcal{B}(B_s \rightarrow K^-\rho^+)$	[7.36, 57.97]	[0.01, 33.31]	[0.01, 31.51]	[15.96, 275.11]	[17.51, 273.01]
$\mathcal{B}(B_s \rightarrow K^{*-}\rho^+)$	[2.47, 127.56]	[1.36, 64.77]	[1.21, 77.47]	[1.21, 72.76]	[1.08, 81.71]
$\mathcal{A}_{CP}(B_s \rightarrow K^-\pi^+)$	[-14.46, 0.97]	[5.00, 25.07]	[5.00, 22.02]	[5.00, 22.73]	[5.00, 19.10]
$\mathcal{A}_{CP}(B_s \rightarrow K^{*-}\pi^+)$	[-4.62, 6.12]	[-12.31, 4.88]	[-20.27, 13.30]	[-5.15, 4.84]	[-4.40, 5.21]
$\mathcal{A}_{CP}(B_s \rightarrow K^-\rho^+)$	[-3.63, 2.03]	[-36.59, 13.70]	[-35.67, 34.38]	[-1.85, 1.48]	[-1.76, 1.26]
$\mathcal{A}_{CP}^{L,dir}(B_s \rightarrow K^{*-}\rho^+)$	[-13.32, 1.62]	[-80.64, 36.23]	[-94.55, 63.70]	[-54.42, 56.75]	[-75.29, 65.98]
$f_L(B_s \rightarrow K^{*-}\rho^+)$	[0.51, 0.98]	[0.02, 0.97]	[0.01, 0.98]	[0.03, 0.98]	[0.01, 0.98]

ties of these direct CPA mostly come from the constrained MI parameters. The uncertainty of $f_L(B_s \rightarrow K^{*-} \rho^+)$ due to different form factors and the constrained MI parameters.

Comparing the SUSY predictions to the SM predictions given in Table 4, we give some remarks on the numerical results:

- The LR and RL MIs have significant effects on $\mathcal{B}(B_s \rightarrow K^- \pi^+)$, and the relevant parameters have been limited by both upper and lower limits of $\mathcal{B}(B_s \rightarrow K^- \pi^+)$ within 2σ ranges. The LR and RL MIs also have great effects on $\mathcal{A}_{CP}^{dir}(B_s \rightarrow K^- \pi^+)$, which could be increased from the SM prediction range $[-0.14, 0.01]$ to about $[0.05, 0.2]$, however, the range $[0.05, 0.2]$ is still far from the central value of its measurement, and is near to the lower limit of the measurement within 2σ ranges. The LR and RL MI parameters just have been limited by the lower limit of $\mathcal{A}_{CP}^{dir}(B_s \rightarrow K^- \pi^+)$ within 2σ ranges.
- The constrained LR insertion still has significant effects on $\mathcal{B}(B_s \rightarrow K^{*-} \pi^+, K^{(*)-} \rho^+)$. The allowed lower limits of $\mathcal{B}(B_s \rightarrow K^{*-} \pi^+, K^- \rho^+)$ could be reduced one or two order(s) from their SM predictions, and the allowed upper limit of $\mathcal{B}(B_s \rightarrow K^{*-} \rho^+)$ has been suppressed a lot from its SM prediction. In the SM, the direct CPA are very small in these decays. It is interesting to find the contributions of the constrained LR insertion have great effects on $\mathcal{A}_{CP}^{dir}(B_s \rightarrow K^{*-} \pi^+, K^{(*)-} \rho^+)$. The allowed ranges of $\mathcal{A}_{CP}^{dir}(B_s \rightarrow K^{*-} \pi^+, K^{(*)-} \rho^+)$ could be extremely enlarged from ones of their tiny SM predictions. We find the constrained LR insertion contributions have a great impact on the longitudinal polarization fraction $f_L(B_s \rightarrow K^{*-} \rho^+)$, which could be reduced to about zero by the constrained LR insertion.
- For the RL MI case, the effects of the constrained RL insertion could exceedingly increase the allowed upper limits of $\mathcal{B}(B_s \rightarrow K^{*-} \pi^+, K^- \rho^+)$ and decrease the upper limit of $\mathcal{B}(B_s \rightarrow K^{*-} \rho^+)$. The RL insertion has small effects on $\mathcal{A}_{CP}^{dir}(B_s \rightarrow K^{*-} \pi^+, K^- \rho^+)$, however, this insertion can greatly affect $\mathcal{A}_{CP}^{L,dir}(B_s \rightarrow K^{*-} \rho^+)$. $f_L(B_s \rightarrow K^{*-} \rho^+)$ also could be reduced to about zero by the constrained RL insertion.

Noted that the LR and RL MIs only generate dipole operators $Q_{7\gamma,8g}$ and $\tilde{Q}_{7\gamma,8g}$, respectively, and $Q_{7\gamma,8g}, \tilde{Q}_{7\gamma,8g}$ do not contribute to the transverse penguin amplitudes at $\mathcal{O}(\alpha_s)$ due to angular momentum conservation in $B_s \rightarrow K^{*-} \rho^+$ decay [51]. In other words, the LR and RL

MIs only contribute to the longitudinal penguin amplitude at $\mathcal{O}(\alpha_s)$. Because the LR and RL contributions are enhanced by $m_{\tilde{g}}/m_b$, even a small $(\delta_{LR}^d)_{13}$ or $(\delta_{RL}^d)_{13}$ can have large effects on the longitudinal penguin amplitude, and then can significantly affect the polarization fractions of $B_s \rightarrow K^{*-} \rho^+$ decay. For the similar reason, the LR and RL MIs have been proposed as a possible resolution to the polarization puzzle in $B \rightarrow \phi K^*$ decays [52, 53].

For each LR and RL insertions, we can present the distributions and correlations of \mathcal{B} , \mathcal{A}_{CP}^{dir} , f_L within the modulus or weak phase of the constrained MI parameter space in Fig. 2 by two-dimensional scatter plots. The LR MI effects on all observables of $B_s \rightarrow K^{(*)-} \pi^+$, $K^{(*)-} \rho^+$ are displayed in Fig. 3 and Fig. 4. Fig. 3 shows the sensitivities of all observables to $|(\delta_{LR}^d)_{13}|$ for different value of x , and we see that all observables except $\mathcal{B}(B_s \rightarrow K^- \pi^+)$ are a little sensitive to both $|(\delta_{LR}^d)_{13}|$ and the values of x . Fig. 4 displays the sensitivities of the observables to ϕ_{LR} for different x , and we can see that the weak phase ϕ_{LR} for different x value has similar allowed ranges, and has similar effects on every observable. In addition, for comparing conveniently, we show the SM bounds of these observables by orange horizontal dash lines and the limits of the measurements of $B_s \rightarrow K^- \pi^+$ within 2σ error-bar by the cyan horizontal solid lines. From Fig. 3(a-d) and Fig. 4(a-d), we see that $\mathcal{B}(B_s \rightarrow K^- \pi^+)$ is strongly constrained from its experimental data, $\mathcal{B}(B_s \rightarrow K^{*-} \pi^+, K^{(*)-} \rho^+)$ are very sensitive to both $|(\delta_{LR}^d)_{13}|$ and ϕ_{LR} , and they are decreasing with $|(\delta_{LR}^d)_{13}|$ but increasing with ϕ_{LR} . As shown in Fig. 3(e) and Fig. 4(e), the LR insertion has positive effects on $\mathcal{A}_{CP}^{dir}(B_s \rightarrow K^- \pi^+)$, and there is no any point in the SM area since $\mathcal{A}_{CP}^{dir}(B_s \rightarrow K^- \pi^+)$ is strongly constrained by the corresponding experimental data, which are not consistent with the SM predictions at 95% C.L.. Fig. 3 (f-h) and Fig. 4 (f-h) display that $\mathcal{A}_{CP}^{dir}(B_s \rightarrow K^{*-} \pi^+, K^{(*)-} \rho^+)$ are sensitive to $|(\delta_{LR}^d)_{13}|$, and could have very large allowed ranges when $\phi_{LR} \in [-80^\circ, -40^\circ]$. As for the LR insertion effects on $f_L(B_s \rightarrow K^{*-} \rho^+)$, we show it in Fig. 3 (i) and Fig. 4 (i), and we can see $f_L(B_s \rightarrow K^{*-} \rho^+)$ could be hugely affected by the LR MI. $f_L(B_s \rightarrow K^{*-} \rho^+)$ has some sensitivities to both $|(\delta_{LR}^d)_{13}|$ and ϕ_{LR} , and it has smaller allowed range with ϕ_{LR} . So the future measurement of $f_L(B_s \rightarrow K^{*-} \rho^+)$ could give obvious constraint on ϕ_{LR} .

Next, we discuss the RL MI effects on all observables in $B_s \rightarrow K^{(*)-} \pi^+$, $K^{(*)-} \rho^+$ decays. Fig. 5 and Fig. 6 show the observables as functions of $|(\delta_{RL}^d)_{13}|$ and ϕ_{RL} , respectively. Fig. 5(a,d) and Fig. 6(a,d) show the constrained RL MI has negative effects on $\mathcal{B}(B_s \rightarrow K^- \pi^+, K^{*-} \rho^+)$,

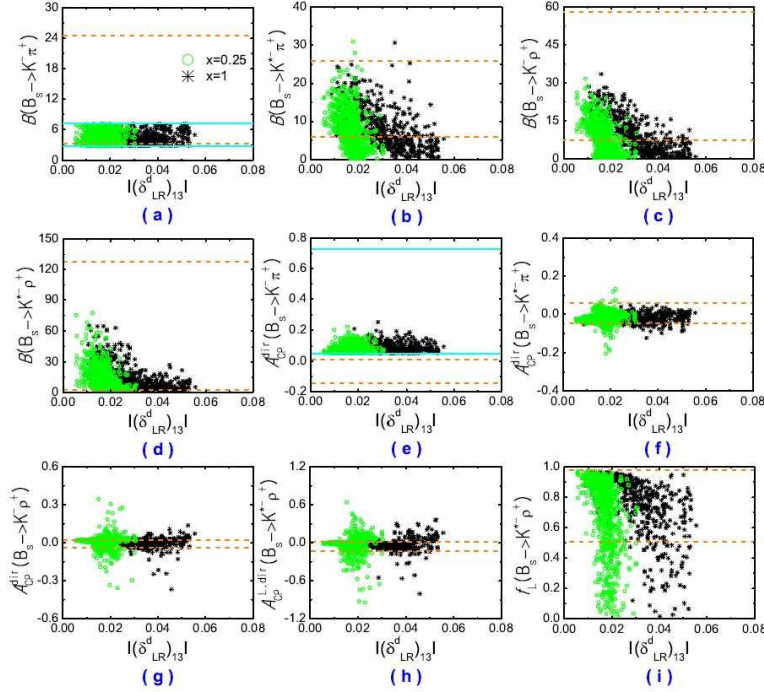


Figure 3: The effects of $|(\delta_{LR}^d)_{13}|$ in $B_s \rightarrow K^{(*)}-\pi^+, K^{(*)}-\rho^+$ decays. \mathcal{A}_{CP}^{dir} and \mathcal{B} are in units of 10^{-2} and 10^{-6} , respectively. The orange horizontal dash lines denote the limits of SM predictions, and the cyan horizontal solid lines represent the 2σ error bar of the measurements. (The same in Figs. 4-6).

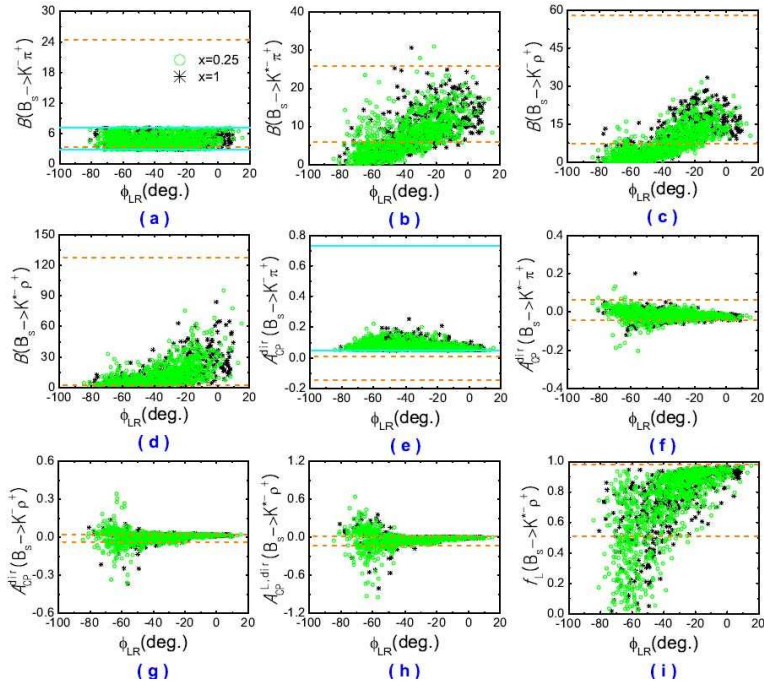


Figure 4: The effects of ϕ_{LR} in $B_s \rightarrow K^{(*)}-\pi^+, K^{(*)}-\rho^+$ decays.

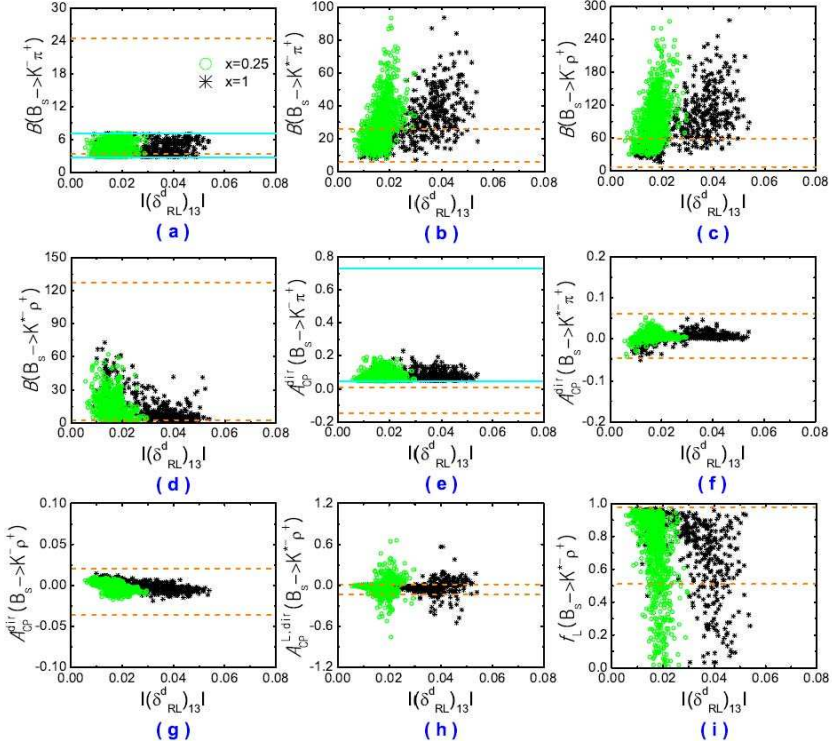


Figure 5: The effects of $|(\delta_{RL}^d)_{13}|$ in $B_s \rightarrow K^{(*)-\pi^+}, K^{(*)-\rho^+}$ decays.

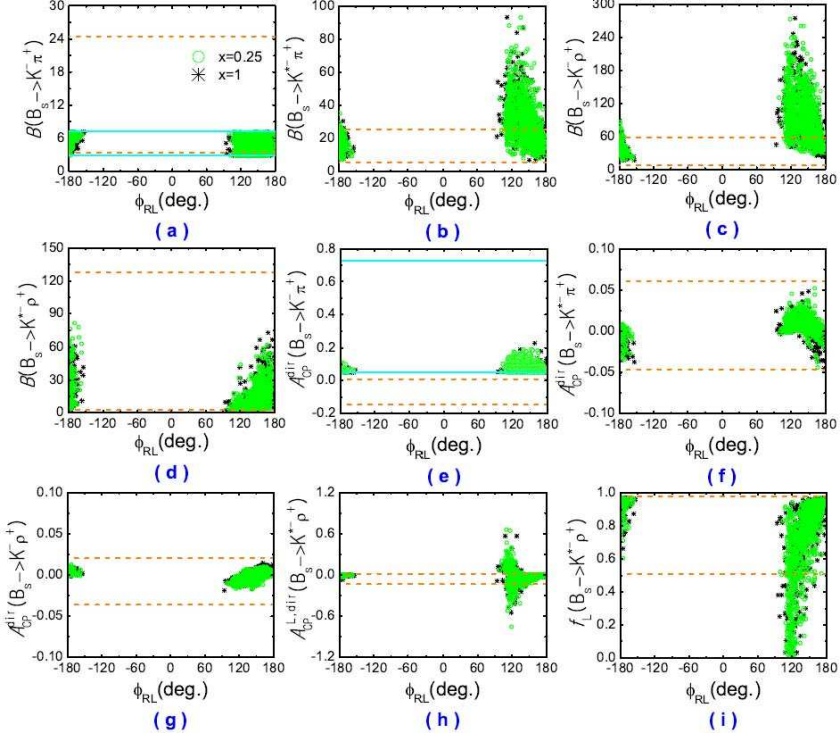


Figure 6: The effects of ϕ_{RL} in $B_s \rightarrow K^{(*)-\pi^+}, K^{(*)-\rho^+}$ decays.

which is same as the LR MI effects on them. Fig. 5(b,c) and Fig. 6(b,c) show us the constrained RL MI has very large positive effects on $\mathcal{B}(B_s \rightarrow K^{*-}\pi^+, K^-\rho^+)$, which is different from the LR MI. $\mathcal{B}(B_s \rightarrow K^{*-}\pi^+, K^{(*)-}\rho^+)$ have some sensitivities to $|(\delta_{RL}^d)_{13}|$ and ϕ_{RL} as displayed in Fig. 5(b-d) and Fig. 6 (b-d). As shown in Fig. 5(f,g) and Fig. 6 (f,g), the RL MI has small effects on $\mathcal{A}_{CP}^{dir}(B_s \rightarrow K^{*-}\pi^+, K^-\rho^+)$, and the RL insertion contributions can not be distinguished from the SM prediction. Fig. 5 (h) and Fig. 6 (h) show the RL MI effects on $\mathcal{A}_{CP}^{dir}(B_s \rightarrow K^{*-}\rho^+)$ are similar to the LR insertion effects on it. $\mathcal{A}_{CP}^{dir}(B_s \rightarrow K^{*-}\rho^+)$ could have very large allowed ranges when $\phi_{RL} \in [100^\circ, 140^\circ]$. As shown in Fig. 6 (i), $f_L(B_s \rightarrow K^{*-}\rho^+)$ could be strongly suppressed by the RL insertion, too.

In addition, for the LR MI case, we show the resulting predictions for $\mathcal{B}(B_s \rightarrow K^-\pi^+)$ vs. $\mathcal{B}(B_s \rightarrow K^{*-}\pi^+, K^{(*)-}\rho^+)$ and $\mathcal{B}(B_s \rightarrow K^-\pi^+)$ vs. $\mathcal{A}_{CP}^{dir}(B_s \rightarrow K^{*-}\pi^+, K^{(*)-}\rho^+)$ in Fig. 7, as well as $\mathcal{A}_{CP}^{dir}(B_s \rightarrow K^-\pi^+)$ vs. $\mathcal{B}(B_s \rightarrow K^{*-}\pi^+, K^{(*)-}\rho^+)$ and $\mathcal{A}_{CP}^{dir}(B_s \rightarrow K^-\pi^+)$ vs. $\mathcal{A}_{CP}^{dir}(B_s \rightarrow K^{*-}\pi^+, K^{(*)-}\rho^+)$ in Fig. 8. In all plots in Fig. 7 and Fig. 8, the black and green points satisfy the constraints of $B_s \rightarrow K^-\pi^+$ decay and $B^0 - \bar{B}^0$ mixing within 2σ ranges. As displayed in Fig. 7, both $\mathcal{B}(B_s \rightarrow K^{*-}\pi^+, K^{(*)-}\rho^+)$ and $\mathcal{A}_{CP}^{dir}(B_s \rightarrow K^{*-}\pi^+, K^{(*)-}\rho^+)$ are not very sensitive to the constrained $\mathcal{B}(B_s \rightarrow K^-\pi^+)$. However, as shown in Fig. 8, both $\mathcal{B}(B_s \rightarrow K^{*-}\pi^+, K^{(*)-}\rho^+)$ and $\mathcal{A}_{CP}^{dir}(B_s \rightarrow K^{*-}\pi^+, K^{(*)-}\rho^+)$ have some sensitivities to the constrained $\mathcal{A}_{CP}^{dir}(B_s \rightarrow K^-\pi^+)$. Fig. 8 (a-c) show us, $\mathcal{A}_{CP}^{dir}(B_s \rightarrow K^-\pi^+)$ could have maximum when $\mathcal{B}(B_s \rightarrow K^{*-}\pi^+, K^{(*)-}\rho^+)$ is near the lower limits of the SM predictions, and $\mathcal{A}_{CP}^{dir}(B_s \rightarrow K^-\pi^+)$ could have smaller allowed range with $\mathcal{B}(B_s \rightarrow K^{*-}\pi^+, K^{(*)-}\rho^+)$. Fig. 8 (d-f) indicate that there are some points accounting for large values of $|\mathcal{A}_{CP}^{dir}(B_s \rightarrow K^{*-}\pi^+, K^{(*)-}\rho^+)|$ when $\mathcal{A}_{CP}^{dir}(B_s \rightarrow K^-\pi^+)$ is small.

There are similar correlations in the case of the RL MI as ones in Fig. 7 and Fig. 8 expect the correlations between $\mathcal{B}(B_s \rightarrow K^-\pi^+)$ and $\mathcal{A}_{CP}^{dir}(B_s \rightarrow K^-\rho^+)$ as well as between $\mathcal{A}_{CP}^{dir}(B_s \rightarrow K^-\pi^+)$ and $\mathcal{A}_{CP}^{dir}(B_s \rightarrow K^{*-}\pi^+, K^-\rho^+)$. $\mathcal{A}_{CP}^{dir}(B_s \rightarrow K^{*-}\pi^+, K^-\rho^+)$ have no any sensitivities to $\mathcal{A}_{CP}^{dir}(B_s \rightarrow K^-\pi^+)$ and $\mathcal{B}(B_s \rightarrow K^-\pi^+)$.

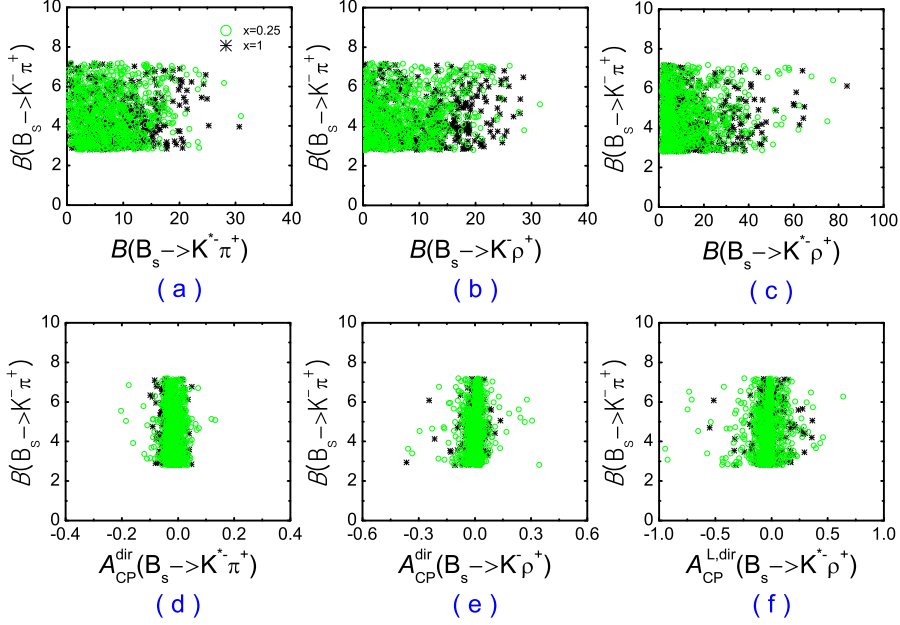


Figure 7: For the LR insertion, the correlation plots between $\mathcal{B}(B_s \rightarrow K^-\pi^+)$ and $\mathcal{B}(B_s \rightarrow K^{*-}\pi^+, K^{(*)-}\rho^+)$ are shown in (a-c), and the correlation plots between $\mathcal{B}(B_s \rightarrow K^-\pi^+)$ and $\mathcal{A}_{CP}^{dir}(B_s \rightarrow K^{*-}\pi^+, K^{(*)-}\rho^+)$ are shown in (d-f).

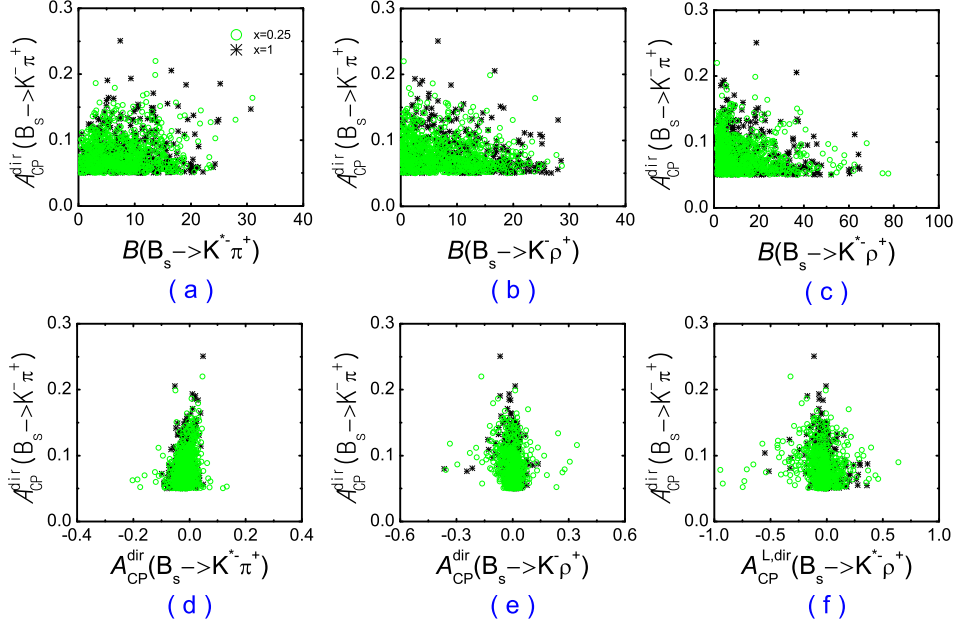


Figure 8: For the LR insertion, the correlation plots between $\mathcal{A}_{CP}^{dir}(B_s \rightarrow K^-\pi^+)$ and $\mathcal{B}(B_s \rightarrow K^{*-}\pi^+, K^{(*)-}\rho^+)$ are shown in (a-c), and the correlation plots between $\mathcal{A}_{CP}^{dir}(B_s \rightarrow K^-\pi^+)$ and $\mathcal{A}_{CP}^{dir}(B_s \rightarrow K^{*-}\pi^+, K^{(*)-}\rho^+)$ are shown in (d-f).

4 Conclusions

Motivated by recent results from CDF, which favor a possible large CP asymmetry and a small branching ratio in $B_s \rightarrow K^-\pi^+$ decay, we have studied the gluino-mediated SUSY contributions with the MIs to four $B_s \rightarrow K^{(*)-}\pi^+, K^{(*)-}\rho^+$ decays based on the QCDF approach. For the LL and RR MIs, we have found that the constrained LL and RR insertion effects from $B^0 - \bar{B}^0$ mixing are almost negligible in $B_s \rightarrow K^{(*)-}\pi^+, K^{(*)-}\rho^+$ decays, hence the LL and RR MIs can not explain the measurements of $B_s \rightarrow K^-\pi^+$ decay from CDF within 2σ ranges. For the LR and RL MIs, we have fairly constrained the LR and RL MI parameters from $B_s \rightarrow K^-\pi^+$ decay and $B^0 - \bar{B}^0$ mixing. Furthermore, using the survived parameter spaces, we have explored the LR and RL MI effects on the observables of three $B_s \rightarrow K^{*-}\pi^+, K^{(*)-}\rho^+$ decays, which have not been measured yet.

The LR and RL insertions can generate sizable effects in $B_s \rightarrow K^{(*)-}\pi^+, K^{(*)-}\rho^+$ decays since their contributions are enhanced by $m_{\tilde{g}}/m_b$. The allowed regions of both the SUSY weak phases $\phi_{LR,RL}$ and the moduli $|(\delta_{LR,RL}^d)_{13}|$ have been strongly constrained from $B_s \rightarrow K^-\pi^+$ decay and $B^0 - \bar{B}^0$ mixing within 2σ ranges. We have found as long as $x \leq 2$, there still is allowed spaces for the LR and RL MI parameters. For $x = 0.25$ case, $B_s \rightarrow K^-\pi^+$ decay and ΔM_d provide the most stringent constraint, however, for $x = 1$ case, $B_s \rightarrow K^-\pi^+$ decay and $\sin 2\beta$ provide the most stringent limit. The theoretical predictions including the constrained LR and RL MI contributions are compatible with the measurements within 2σ ranges from CDF collaboration in $B_s \rightarrow K^-\pi^+$ decay. We have found the constrained LR and RL insertions still have obvious effects on $\mathcal{B}(B_s \rightarrow K^{*-}\pi^+, K^{(*)-}\rho^+)$, $\mathcal{A}_{CP}^{L,dir}(B_s \rightarrow K^{*-}\rho^+)$ and $f_L(B_s \rightarrow K^{*-}\rho^+)$, moreover, the LR insertion has obvious effects on $\mathcal{A}_{CP}^{dir}(B_s \rightarrow K^-\rho^+)$. Then we have presented the sensitivities of the physical observable quantities to the constrained LR and RL parameter spaces in Figs. 3-6. We have found $\mathcal{A}_{CP}^{dir}(B_s \rightarrow K^-\rho^+, K^{*-}\rho^+)$ and $f_L(B_s \rightarrow K^{*-}\rho^+)$ are very sensitive to the weak phases of the LR and RL insertion parameters. In addition, we also have shown the correlations between two observables of $B_s \rightarrow K^-\pi^+$ decay and the observables of $B_s \rightarrow K^{*-}\pi^+, K^{(*)-}\rho^+$ decays in Figs. 7-8. And we have found all observables of $B_s \rightarrow K^{*-}\pi^+, K^{(*)-}\rho^+$ decays are not very sensitive to $\mathcal{B}(B_s \rightarrow K^-\pi^+)$ for the LR and RL MIs, $\mathcal{B}(B_s \rightarrow K^{*-}\pi^+, K^{(*)-}\rho^+)$ and $\mathcal{A}_{CP}^{dir}(B_s \rightarrow K^{*-}\rho^+)$ have some sensitivities to $\mathcal{A}_{CP}^{dir}(B_s \rightarrow K^-\pi^+)$ in the case of the LR and RL MIs, and $\mathcal{A}_{CP}^{dir}(B_s \rightarrow K^{*-}\pi^+, K^-\rho^+)$ are

also sensitive to $\mathcal{A}_{CP}^{dir}(B_s \rightarrow K^-\pi^+)$ for the LR MI case. The future measurements or precise measurements of the branching ratios, the direct CP asymmetries and the polarization fractions in $B_s \rightarrow K^{(*)-}\pi^+, K^{(*)-}\rho^+$ decays could be used to shrink/reveal/rule out the relevant LR and RL MI parameter spaces. The results in this paper could be useful for probing SUSY effects and searching direct SUSY signals at Tevatron and LHC in the near future.

References

- [1] A. Abulencia *et al.* [CDF Collaboration], Phys. Rev. Lett. **97**, 211802 (2006) [arXiv:hep-ex/0607021].
- [2] M. Morello [CDF Collaboration], arXiv:0810.3258 [hep-ex].
- [3] T. Aaltonen *et al.* [CDF Collaboration], Phys. Rev. Lett. **103**, 031801 (2009), arXiv:0812.4271 [hep-ex].
- [4] [CDF Collaboration], “Measurement of branching fractions and direct CP asymmetries of $B_{(s)}^0 \rightarrow h^+h^-$ decays in 1fb^{-1} ,” and the updated results on April 10, 2008 may be found on <http://www-cdf.fnal.gov/physics/new/bottom/bottom.html> [Note 8579v1].
- [5] A. R. Williamson and J. Zupan, Phys. Rev. D **74**, 014003 (2006) [Erratum-ibid. D **74**, 03901 (2006)] [arXiv:hep-ph/0601214].
- [6] M. Beneke and M. Neubert, Nucl. Phys. B **675**, 333 (2003) [arXiv:hep-ph/0308039].
- [7] A. Ali *et al.*, Phys. Rev. D **76**, 074018 (2007) [arXiv:hep-ph/0703162].
- [8] M. Beneke, G. Buchalla, M. Neubert and C. T. Sachrajda, Phys. Rev. Lett. **83**, 1914 (1999) [arXiv:hep-ph/9905312]; Nucl. Phys. B **591**, 313 (2000) [arXiv:hep-ph/0006124]; Nucl. Phys. B **606**, 245 (2001) [arXiv:hep-ph/0104110].
- [9] Y. Y. Keum, H. n. Li and A. I. Sanda, Phys. Lett. B **504**, 6 (2001) [arXiv:hep-ph/0004004]; Phys. Rev. D **63**, 054008 (2001) [arXiv:hep-ph/0004173]; Y. Y. Keum and H. n. Li, Phys. Rev. D **63**, 074006 (2001) [arXiv:hep-ph/0006001]; C. D. Lü, K. Ukai and M. Z. Yang, Phys. Rev. D **63**, 074009 (2001)

- [arXiv:hep-ph/0004213]; Y. Y. Keum and A. I. Sanda, Phys. Rev. D **67**, 054009 (2003) [arXiv:hep-ph/0209014].
- [10] C. W. Bauer, S. Fleming and M. E. Luke, Phys. Rev. D **63**, 014006 (2000) [arXiv:hep-ph/0005275]; C. W. Bauer, S. Fleming, D. Pirjol and I. W. Stewart, Phys. Rev. D **63**, 114020 (2001) [arXiv:hep-ph/0011336]; C. W. Bauer and I. W. Stewart, Phys. Lett. B **516**, 134 (2001) [arXiv:hep-ph/0107001].
- [11] M. Gronau and J. L. Rosner, Phys. Lett. B **482**, 71 (2000) [arXiv:hep-ph/0003119].
- [12] H. J. Lipkin, Phys. Lett. B **621**, 126 (2005) [arXiv:hep-ph/0503022].
- [13] M. Beneke, J. Rohrer and D. Yang, Nucl. Phys. B **774**, 64 (2007) [arXiv:hep-ph/0612290].
- [14] C. H. Chen, Phys. Lett. B **520**, 33 (2001) [arXiv:hep-ph/0107189].
- [15] X. Li, G. Lu and Y. D. Yang, Phys. Rev. D **68**, 114015 (2003) [Erratum-ibid. D **71**, 019902 (2005)] [arXiv:hep-ph/0309136].
- [16] Y. G. Xu, R. M. Wang and Y. D. Yang, Phys. Rev. D **79**, 095017 (2009), arXiv:0903.0256 [hep-ph].
- [17] H. Y. Cheng and C. K. Chua, arXiv:0910.5237 [hep-ph].
- [18] S. W. Lin *et al.* [Belle Collaboration], Nature **452**, 332 (2008).
- [19] B. Aubert *et al.* [BABAR Collaboration], Phys. Rev. Lett. **99**, 021603 (2007) [arXiv:hep-ex/0703016].
- [20] K. Abe *et al.* [Belle Collaboration], Phys. Rev. Lett. **93**, 021601 (2004) [arXiv:hep-ex/0401029].
- [21] B. Aubert *et al.* [BABAR Collaboration], Phys. Rev. Lett. **95**, 151803 (2005) [arXiv:hep-ex/0501071].
- [22] B. Aubert *et al.* [BABAR Collaboration], arXiv:0807.4226 [hep-ex].
- [23] S. Baek, JHEP **0607**, 025 (2006) [arXiv:hep-ph/0605094];

- [24] Y. D. Yang, R. Wang and G. R. Lu, Phys. Rev. D **73**, 015003 (2006) [arXiv:hep-ph/0509273].
- [25] A. J. Buras, R. Fleischer, S. Recksiegel and F. Schwab, Acta Phys. Polon. B **36**, 2015 (2005) [arXiv:hep-ph/0410407].
- [26] L. J. Hall, V. A. Kostelecky and S. Raby, Nucl. Phys. B **267**, 415 (1986).
- [27] F. Gabbiani, E. Gabrielli, A. Masiero and L. Silvestrini, Nucl. Phys. B **477**, 321 (1996) [arXiv:hep-ph/9604387].
- [28] F. Gabbiani and A. Masiero, Nucl. Phys. B **322**, 235 (1989).
- [29] J. S. Hagelin, S. Kelley and T. Tanaka, Nucl. Phys. B **415** (1994) 293.
- [30] E. Gabrielli, A. Masiero and L. Silvestrini, Phys. Lett. B **374**, 80 (1996) [arXiv:hep-ph/9509379].
- [31] G. Buchalla, A. J. Buras and M. E. Lautenbacher, Rev. Mod. Phys. **68**, 1125 (1996) [arXiv:hep-ph/9512380].
- [32] S. Baek, J. H. Jang, P. Ko and J. h. Park, Nucl. Phys. B **609**, 442 (2001) [arXiv:hep-ph/0105028].
- [33] G. L. Kane *et al.*, Phys. Rev. D **70**, 035015 (2004) [arXiv:hep-ph/0212092].
- [34] D. K. Ghosh, X. G. He, Y. K. Hsiao and J. Q. Shi, [arXiv:hep-ph/0206186].
- [35] A. J. Buras *et al.*, Nucl. Phys. B **566**, 3 (2000) [arXiv:hep-ph/9908371].
- [36] X. G. He, J. Y. Leou and J. Q. Shi, Phys. Rev. D **64**, 094018 (2001) [arXiv:hep-ph/0106223].
- [37] A. L. Kagan, [arXiv:hep-ph/0407076].
- [38] D. Becirevic *et al.*, Nucl. Phys. B **634**, 105 (2002) [arXiv:hep-ph/0112303].
- [39] E. Barberio *et al.* [Heavy Flavor Averaging Group], arXiv:0808.1297 [hep-ex].

- [40] M. Artuso *et al.*, Eur. Phys. J. C **57**, 309 (2008), arXiv:0801.1833 [hep-ph].
- [41] W. Altmannshofer, A. J. Buras, S. Gori, P. Paradisi and D. M. Straub, arXiv:0909.1333 [hep-ph].
- [42] P. Ko, J. h. Park and G. Kramer, Eur. Phys. J. C **25**, 615 (2002) [arXiv:hep-ph/0206297].
- [43] C. Amsler *et al.* [Particle Data Group], Phys. Lett. B **667**, 1 (2008) and 2009 partial update for the 2010 edition.
- [44] M. Bona *et al.* (UT fitter Group), <http://www.utfit.org/>.
- [45] P. Ball and R. Zwicky, Phys. Rev. D **71**, 014015 (2005) [arXiv:hep-ph/0406232]; Phys. Rev. D **71**, 014029 (2005) [arXiv:hep-ph/0412079].
- [46] G. Duplancic and B. Melic, Phys. Rev. D **78**, 054015 (2008), arXiv:0805.4170 [hep-ph].
- [47] V. Lubicz and C. Tarantino, Nuovo Cim. **123B**, 674 (2008), arXiv:0807.4605 [hep-lat].
- [48] V. M. Braun, D. Y. Ivanov and G. P. Korchemsky, Phys. Rev. D **69**, 034014 (2004) [arXiv:hep-ph/0309330].
- [49] A. J. Buras, M. Jamin and P. H. Weisz, Nucl. Phys. B **347**, 491(1990); J. Urban *et al.*, Nucl. Phys. B **523**, 40(1998).
- [50] D. Bećirević *et al.*, JHEP **0204**, 025(2002).
- [51] A. L. Kagan, Phys. Lett. B **601**, 151 (2004) [arXiv:hep-ph/0405134].
- [52] C. S. Huang, P. Ko, X. H. Wu and Y. D. Yang, Phys. Rev. D **73**, 034026 (2006) [arXiv:hep-ph/0511129].
- [53] A. K. Giri and R. Mohanta, arXiv:hep-ph/0412107.